The Stress Response of Electrorheological Core-Shell and Hard-Core Suspensions upon the Frequency of External Fields

I-Chung Cheng[*], Woei-Shyong Lee[**], Chang Chuen Sun[***], and Wen-Hwa Hwu[*]

[*]*Department of Applied Chemistry, Chung Cheng Institute of Technology, National Defense University*
[**]*Mackay Medicine, Nursing and Management College*
[***]*Department of Electronic Engineering, Lee-Ming Institute of Technology*

ABSTRACT

The theoretical investigation of the stress response influenced by an electric field frequency has been studied for suspended particles with a core-shell and hard core structures, respectively, in an electrorheological fluid (ERF). The dielectric constant and material conductivity are considered in the model. The relationship between the stress and frequency under the AC field effect is obtained using the point-dipole approximation method. The electric potential is solved using Laplace's equation. The computational results confirmed that the external field can be appropriately chosen and applied to an ERF system involving particles with the recommended structures dispersed in an insulating fluid.

Keywords: electrorheological fluid, field frequency, stress response, point-dipole approximation

電場頻率影響電流變流體核殼與實心結構懸浮粒子之應力應答理論研究

鄭義忠[*] 李偉雄[**] 孫長春[***] 胡文華[*]

[*]國防大學中正理工學院應用化學研究所
[**]馬偕醫護管理專科學校
[***]黎明技術學院電子工程系

摘　　要

本文從理論上分別探討實心粒子與核殼結構粒子的應力對電場頻率的應答情形。考慮材料的介電係數和導電率，在交流電場作用下，解 Laplace 方程式並採用點偶極近求得電位分佈，並進而獲得應力與電場頻率間的關係。由計算結果得知，藉由所得關係可於電流變液懸浮粒子於正式運用時，決定外部電場環境的選用。

關鍵詞：電流變流體，電場頻率，應力應答，點偶極近似

文稿收件日期 94.2.15. ; 文稿修正後接受日期 94.8.10.
Manuscript received Feb.15, 2005 ; revised Aug. 10, 2005.

I. INTRODUCTION

An electrorheological fluid (ERF) is a smart fluid whose viscosity and yield stress can be controlled by applying an electric field. The advantages of ER fluids are quick response to an action, simple structures, and low energy consumption. Although ER fluids were discovered in 1949 by Winslow, after half a century, ER elements are still in the development stage for commercial purposes [1]. The main reason why ER fluids are still not widely used is that the yield stress is not high enough and the ER system is not yet wholly stable [2].

Early theoretical studies on the interaction force between two adjacent particles in an electrorheological (ER) suspension employed the point-dipole approximation, assuming that no electric current flowed through the suspension [3-5]. The coordinate system used to define the pair interaction due to electrical polarization is shown in Figure 1. The interaction force is given in Equation 1.

$$\vec{F}_{ij}(r,\theta) = \frac{3p^2}{4\pi\varepsilon_f}\frac{1}{r^4}\left[\left(3\cos^2\theta - 1\right)\vec{a}_r + \left(\sin 2\theta\right)\vec{a}_\theta\right] \quad (1)$$

where

$$p = 4\pi\varepsilon_f \beta b^3 E_o \quad (2)$$

$$\beta = \frac{\alpha - 1}{\alpha + 2}; \qquad \alpha = \frac{\varepsilon_p}{\varepsilon_f} \quad (3a,b)$$

and p is the dipole moment, b the particle radius, ε_f the permittivity of the insulating fluid, ε_p the permittivity of the particle, E_o the external electric field, r the distance between two particle centers, $\vec{a}_r$, $\vec{a}_\theta$ the spherical coordinate unit electric field, r the distance between two particle vectors in the r and θ directions, respectively. The derivation of the dipole moment, p, described in Equation (2) is listed in Appendix.

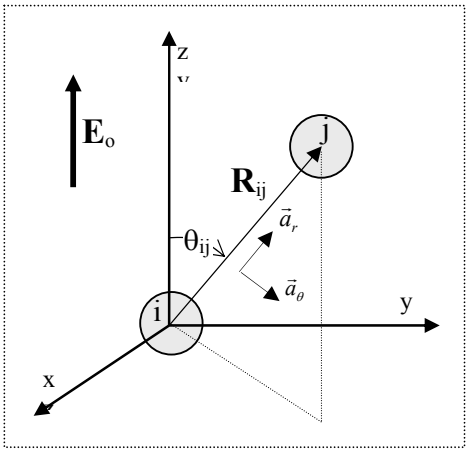

Fig 1. Coordinate system used to define the pair interaction due to electrical polarization [Eq. 1]. E_o is the external electric field.

Equation 1 is only suitable for the case involving two polarized particles separated far away from each other. Once two polarized particles are very close, they will affect one another. Ultimately, they will become polarized and much further apart. The polarization of both particles increases and the inter-force between the two particles also increases. Therefore, the point-dipole approximation gives the inter-particle force an order of magnitude lower than that observed. Previous investigators proposed modifications to the polarization model for predicting the inter-particle force. Their computational predictions were much closer to the observed values [3, 5-10]. Among these modifications, the corrected polarization model using the Maxwell-Wagner polarization was proposed to take the conductivities of the materials into account for predicting the interaction force between particles. The conductivities of the particles and host liquids can be included in the polarization model using the complex permittivity, namely

$$\beta^* = \frac{\alpha^* - 1}{\alpha^* + 2}; \quad \alpha^* = \frac{\varepsilon_p^*}{\varepsilon_f^*} = \frac{K_p - i\frac{\sigma_p}{\omega\varepsilon_o}}{K_f - i\frac{\sigma_f}{\omega\varepsilon_o}} \quad (4a,b)$$

where β^* is called the Clausius-Mossotti factor, ω is the field frequency, ε_o the permittivity of a vacuum, ε the permittivity of the materials, K the relative permittivity of the materials and σ the conductivity of the materials. The subscripts p and f refer to the particles and the insulating fluid, respectively. When the electrical field frequency ω is very high, Equation 4b is reduced to Equation 3b. When the field frequency ω is very low, Equation 4b is reduced to

$$\alpha^* = \frac{\sigma_p}{\sigma_f} \quad (5)$$

The stress response behavior of an electrorheological fluid is dominated by different material parameters, such as the conductivity ratio or dielectric constant ratio, under a DC or AC field.

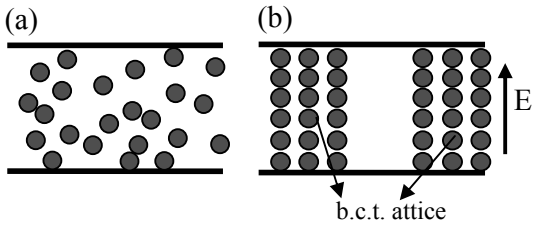

Fig. 2. Schematic illustration of the structure change of an ERF before (a) and after(b) an external electric field is applied.

The particle fabrication technique has been significantly improved in recent years, especially for making composite spheres and powders. To produce a higher ERF stress response, ERF dispersing particles with various structures were studied. Among these structures, a core-shell structure was emphasized, such as an inorganic core with a semi-conducting polymeric shell [11-16], a polymeric core with a semi-conducting polymeric shell [2, 17, 18], and a metallic core with an inorganic shell [19, 20].

The ERF owns extraordinary rheological properties, such as induced yield stress, abrupt liquid viscosity increase. They are strongly related to the structure variation influenced by an external field. Figure 2 is the structure change diagram of a ERF system affected before and after an external field application. Before the electric field is applied, the particulates are randomly distributed in ER system. After an external field is applied, the dispersed particulates oriented to form chains along the direction of the applied field. Between two electrode plates, the larger the chain number is and the stronger the chain interforces are, the larger the yield stress and viscosity of the ERF owns. The chain number is determined from the volume fraction and the chain interforces are determined from the polarization interaction. The interforces are affected by choosing material choices and electric field, either DC or AC. Therefore, from the microscopic viewpoint, as long as the solid particles produce large interaction forces among particles after polarization, the ER system will have high yield stress.

In this study, we discuss the inter-particle force affected by the electric field frequency and material parameters for core-shell particles using Maxwell-Wagner polarization. The predicted results are useful information in the fabrication of ERF particles and in the proper external electric field choice, DC or AC field.

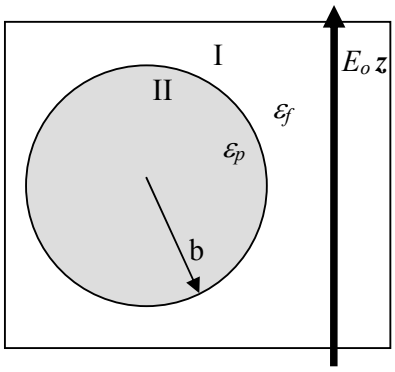

Fig. 3. Schematic drawing of a particle with a single phase, where *b* is the radius of the particle (I: oil zone, II: particle zone).

II. MATHEMATICAL MODEL

2.1 Hard Core Particles

The Maxwell-Wagner model described particle polarization accounting for both the particle and bulk fluid conductivities, as well as their permittivities [21, 22]. In this model, the permittivity and conductivity of individual phases are assumed to be constant and independent of the frequency. The complex dielectric constants of the disperse and fluid phases are written as $\varepsilon_m^*(\omega_e) = K_m - j\frac{\sigma_m}{\omega_e \varepsilon_o}$, where m=p, f, $j = \sqrt{-1}$, the asterisks represent complex quantities, and ω_e the electrical field frequency.

Considering an isolated sphere with a single solid phase in a uniform AC electric field, $\mathbf{E_o} = \mathrm{Re}\{E_o e^{j\omega_e t}\mathbf{e_z}\}$, the complex potential satisfies Laplace's equation in the bulk phases [21], $\nabla^2 V^* = 0$, and subject to the boundary conditions at the interface, referring to Figure 3,

$$V^{*I} = V^{*II} \tag{6a}$$

$$\varepsilon_f^* \nabla V^{*I} \cdot \mathbf{n} = \varepsilon_p^* \nabla V^{*II} \cdot \mathbf{n} \tag{6b}$$

where **n** is a unit vector normal to the surface. The solution for the complex potential resembles that for the ideal case,

$$V^{*II} = -E_o r \frac{3\varepsilon_f^*}{\varepsilon_p^* + 2\varepsilon_f^*} \cos\theta \, e^{j\omega_e t} \tag{7}$$

$$V^{*I} = -E_o r\left[1-\beta^*\left(\frac{b}{r}\right)^3\right]\cos\theta\, e^{j\omega_e t} \tag{8}$$

where

$$\beta^* = \frac{\alpha^*-1}{\alpha^*+2}\ ;\ \alpha^* = \frac{\varepsilon_p^*}{\varepsilon_f^*} \tag{9a,b}$$

The time-averaged force on a sphere at the origin against a second sphere at (R, θ) may be determined easily in the point-limit as before,

$$\vec{F}_{ij}(r,\theta) = \left[\frac{\omega_e}{2\pi}\int_0^{\frac{2\pi}{\omega_e}}\left(\vec{F}_{ij}^{\,*}(r,\theta)\right)^2 dt\right]^{\frac{1}{2}} \tag{10}$$

$$= \frac{3p_{eff}^2}{4\pi\varepsilon_f}\frac{1}{r^4}\left[\left(3\cos^2\theta-1\right)\vec{a}_r + \left(\sin 2\theta\right)\vec{a}_\theta\right]$$

where

$$\vec{F}_{ij}^{\,*}(r,\theta) = \left[\left(\vec{p}_i^{\,*}\cdot\nabla\right)E_j^{\,*}\right]_{x=0} \tag{11a}$$

$$p_{eff}^2 = \left(4\pi\varepsilon_f b^3\right)^2 E_{rms}^2\beta_{eff}^2(\omega_e)\ ;\ E_{rms} = \frac{E_o}{\sqrt{2}} \tag{11b,c}$$

In Equations 10 and 11, subscripts *eff* represent the effective quantity and E_{rms} is a root mean square electric field which is a time-averaged value. In Equation 11, the term, $\beta_{eff}(\omega_e)$, is called "effective relative polarizability". The square of the effective relative polarizability, $\beta_{eff}^2(\omega_e) = \overline{\beta}^*\beta^*$, that is

$$\beta_{eff}^2(\omega_e) = \beta_d^2\frac{\left[\left(\omega_e t_{mw}\right)^2+\frac{\beta_c}{\beta_d}\right]^2+\left(\omega_e t_{mw}\right)^2\left[1-\frac{\beta_c}{\beta_d}\right]^2}{\left[1+\left(\omega_e t_{mw}\right)^2\right]^2} \tag{12}$$

where

$$t_{mw} = \varepsilon_o\frac{K_p+2K_f}{\sigma_p+2\sigma_f}\ ;\ \beta_c = \frac{\sigma_p-\sigma_f}{\sigma_p+2\sigma_f}\ ; \tag{13a,b}$$

$$\beta_d = \frac{K_p-K_f}{K_p+2K_f} \tag{13c}$$

Equation 12 can be rearranged to

$$\beta_{eff}^2(\omega_e) = \frac{\left(\omega_e t_{mw}\right)^2\beta_d^2+\beta_c^2}{1+\left(\omega_e t_{mw}\right)^2} \tag{14}$$

The inter-force is essentially equivalent to the ideal case except that the effective relative polarizability is a function of the field frequency, as well as the permittivities and conductivities of both phases. The value of $\beta_{eff}^2(\omega_e)$, and thus the pair force, depends on the frequency relative to the polarization time constant t_{mw}. In the limit of large frequencies, permittivities dominate the response,

$$\lim_{\omega_e t_{mw}\to\infty}\beta_{eff}^2(\omega_e) = \beta_d^2 \tag{15}$$

While in the DC limit, conductivities control particle polarization forces, regardless of the permittivities.

$$\lim_{\omega_e t_{mw}\to 0}\beta_{eff}^2(\omega_e) = \beta_c^2 \tag{16}$$

2.2 Core-Shell Particles

A core-shell structure was chosen in this study based on the Maxwell-Wagner model. A schematic drawing of a particle with a core-shell structure is shown in Figure 4. The electrical potential satisfies Laplace's equation $\nabla^2 V = 0$ for the insulating oil zone (zone I), shell zone (zone II), and core zone (zone III), respectively. The potentials at the surface and the interface of the sphere are continuous so that there are six boundary conditions

$$\begin{aligned} &r\to\infty \quad V^{*I} = -E_o^* r\cos\theta \\ &r = b \quad V^{*I} = V^{*II},\ \varepsilon_f^*\nabla V^{*I}\cdot n = \varepsilon_p^*\nabla V^{*II}\cdot n \\ &r = a \quad V^{III} = V^{II},\ \varepsilon_{pi}^*\nabla V^{*III}\cdot n = \varepsilon_p^*\nabla V^{*II}\cdot n \\ &r = 0 \quad V^{III} = finite \end{aligned} \tag{17}$$

Equation 18 is a general expression for the electrical potential distribution of the particle in zone I by solving Laplace's equation associated with the boundary conditions, Equation 17.

$$V^{*I} = -E_o r\left[1-\beta^*\left(\frac{b}{r}\right)^3\right]\cos\theta\, e^{j\omega_e t}\ ;\ r\ge b \tag{18}$$

where

$$\beta^* = \frac{b^3\left(2\varepsilon_2^*+1\right)\left(\varepsilon_1^*-1\right)-a^3\left(\varepsilon_2^*-1\right)\left(2\varepsilon_1^*+1\right)}{b^3\left(2\varepsilon_2^*+1\right)\left(\varepsilon_1^*+2\right)-2a^3\left(\varepsilon_2^*-1\right)\left(\varepsilon_1^*-1\right)} \tag{19a}$$

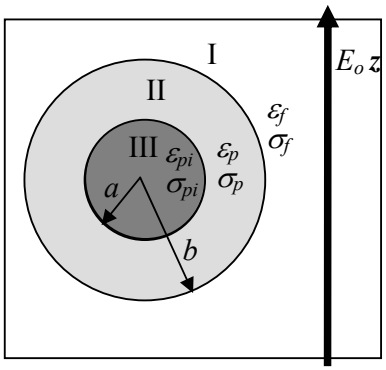

Fig. 4. Schematic drawing of a particle with a core-shell structure. The thickness of the shell is *b*-*a*, where *b* is the radius of the particle and *a* is the radius of the inner core (I: oil zone, II: shell zone, III: core zone).

$$\varepsilon_1^* = \frac{\varepsilon_p^*}{\varepsilon_f^*} \;;\; \varepsilon_2^* = \frac{\varepsilon_p^*}{\varepsilon_{pi}^*} \tag{19b,c}$$

For convenience, Equation 19a is rearranged as

$$\beta^* = \frac{\alpha^* - 1}{\alpha^* + 2} \tag{20a}$$

$$\alpha^* = \varepsilon_1^* \frac{K^* - 2}{K^* + 1} \;;\; K^* = \left(\frac{b}{a}\right)^3 \left(\frac{2\varepsilon_2^* + 1}{\varepsilon_2^* - 1}\right) \tag{20b,c}$$

In Equation 19c, when $\varepsilon_2^* = 1$, the conductivity of the core and shell materials is the same or the structure has no core, a=0. Thus, the α^* in Equation 20b can be simplified into Equation 9b. Comparing Equation 9b to 20b, for the case of $\varepsilon_2^* \neq 1$, the α^* in the core-shell structure has one more factor, (K^*-2)/(K^*+1), than the α^* in the hard core case. This factor is a function of the particle structure, the ratio of the shell material complex conductivity to the complex conductivity of the core material. The β_{eff}^2 of core-shell particles was calculated using square of effective relative polarizability, $\beta_{eff}^2(\omega_e) = \overline{\beta}^* \beta^*$. In the limit of large frequencies, permittivities dominate the response,

$$\lim_{\omega_e \to \infty} \beta_{eff}^2(\omega_e) = \beta_{d,CS}^2 \tag{21}$$

where

$$\beta_{d,CS}^2 = \left[\frac{b^3(2\varepsilon_2 + 1)(\varepsilon_1 - 1) - a^3(\varepsilon_2 - 1)(2\varepsilon_1 + 1)}{b^3(2\varepsilon_2 + 1)(\varepsilon_1 + 2) - 2a^3(\varepsilon_2 - 1)(\varepsilon_1 - 1)}\right]^2 \tag{22a}$$

$$\varepsilon_1 = \frac{K_p}{K_f} \;;\; \varepsilon_2 = \frac{K_p}{K_{pi}} \tag{22b,c}$$

While in the DC limit, conductivities control particle polarization forces.

$$\lim_{\omega_e \to \infty} \beta_{eff}^2(\omega_e) = \beta_{c,CS}^2 \tag{23}$$

where

$$\beta_{c,CS}^2 = \left[\frac{b^3(2\sigma_2 + 1)(\sigma_1 - 1) - a^3(\sigma_2 - 1)(2\sigma_1 + 1)}{b^3(2\sigma_2 + 1)(\sigma_1 + 2) - 2a^3(\sigma_2 - 1)(\sigma_1 - 1)}\right]^2 \tag{24a}$$

$$\sigma_1 = \frac{\sigma_p}{\sigma_f} \;;\; \sigma_2 = \frac{\sigma_p}{\sigma_{pi}} \tag{24b,c}$$

III. RESULTS AND DISCUSSION

3.1 Hard Core Particles

β_c and β_d, appearing in Equations 12 to 14, are either positive or negative. Both depend on positive or negative numerator terms, $\sigma_p - \sigma_f$ and $K_p - K_f$, appearing in Equations 13b and 13c. However, the value of the normalized polarization force magnitude, $\beta_{eff,norm}^2$, is determined by the absolute values of β_c and β_d. The β_{eff}^2 and $\beta_{eff,norm}^2$ are plotted as a function of the frequency in Figure 5 for different values of $|\beta_c|$ and $|\beta_d|$. From Figure 5a, $\beta_{eff,norm}^2$ is independent of the frequency when $|\beta_c|$ is equal

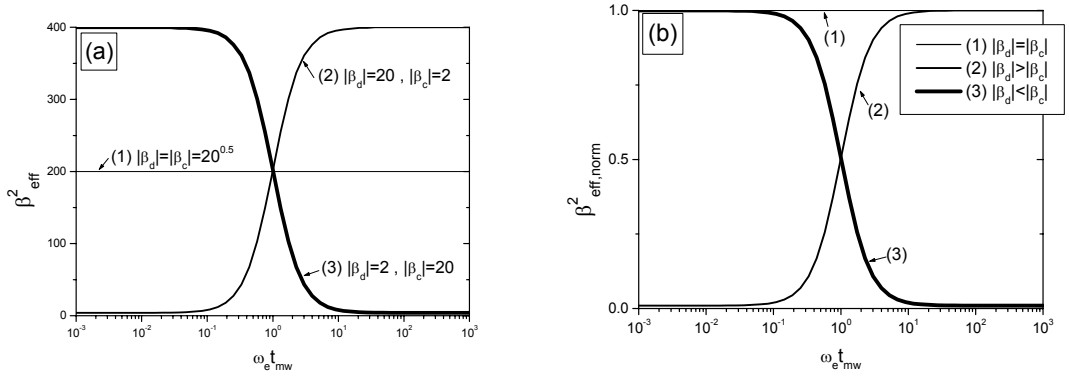

Fig. 5. (a) Square of the effective relative polarizabizaility, β_{eff}^2, and (b) the normalized polarization force magnitude, $\beta_{eff,norm}^2$, as a function of the dimensionless frequency in the Maxwell-Wagner formalism for a particle with a single solid phase. ω_e is the frequency of the applied electric field and t_{mw} is the polarization time constant.

to $|\beta_d|$. While $|\beta_c|$ is not equal to $|\beta_d|$, $\beta^2_{eff,norm}$ changes abruptly in the range of $0.1 < \omega_e t_{mw} < 10$. A reflection point exists and its corresponding frequency is denoted as ω_{ei}. When we choose amaterial whose $|\beta_d|$ is greater than $|\beta_c|$, $\beta^2_{eff,norm}$ increases with the electrical field frequency increasing. On the contrary, when a material with $|\beta_d| < |\beta_c|$ is chosen, $\beta^2_{eff,norm}$ decreases when the electrical field frequency increases. This likely explains, qualitatively, why high dielectric constant materials such as barium titanate ($\varepsilon_p \approx O(10^3)$) do not show a very large ER effect in DC fields, and why many systems exhibit a decrease in apparent viscosity with increasing electric frequency [23-26].

Should a DC or AC field be chosen as the external electrical field for the hard core particles in ERF practical applications? The answer to this question is implied in Figure 5b. Three suggestions are provided

(1) To have maximum interaction forces, it is recommended that an AC electric field be used with an ERF field and that a frequency be applied with a magnitude one order higher than ω_{ei} if $|\beta_d| > |\beta_c|$.

(2) If $|\beta_d| < |\beta_c|$, in order to have maximum interaction forces, it is recommended ERF that a DC electric field be used with the ERF system. However, if an AC filed is used, it is recommended that a frequency with a magnitude one order lower than ω_{ei} be applied to the ERF system.

(3) If one wants to change the interaction forces by changing the frequency, the frequency must fall in the range of $0.1 < \omega_e t_{mw} < 10$. Therefore, a frequency corresponding to the reflection point must be precisely determined. The frequency, ω_{ei}, can be obtained by differentiating Equation 14 twice with respect to $\omega_e t_{mw}$ and let it be zero. The frequency is

$$\omega_{ei} = \sqrt{\frac{1}{3}}\frac{1}{t_{mw}} = \sqrt{\frac{1}{3}}\frac{\sigma_p + 2\sigma_f}{\varepsilon_o\left(K_p + 2K_f\right)} \tag{25}$$

To fabricate an ERF, the frequency range can be determined using Equation 25 as long as the dielectric constants and conductivities of the particles and the surrounding medium are known. In addition, using the definition of $\sigma_1 = \sigma_p / \sigma_f$ and $\varepsilon_1 = K_p / K_f$, Equation 25 can be rewritten as

$$\omega_{ei} = \sqrt{\frac{1}{3}}\frac{\sigma_f}{\varepsilon_o K_f}\frac{\sigma_1 + 2}{\varepsilon_1 + 2} \tag{26}$$

Once the surrounding medium is chosen, the frequency at the reflection point, ω_{ei}, will change with the conductivity ratio of the particle to the medium, σ_1, and the dielectric ratio of the particle to the medium, σ_1. From Equation 26, ω_{ei} increases with σ_1 increasing, while ω_{ei} decreases with ε_1 increasing.

3.2 Core-Shell Particles

In the case of hard core particles, β^2_{eff} is concisely expressed by electric parameters $\omega_e t_{mw}$, β_c and β_d. It is easy to analytically solve the frequency at the reflection point simply by differentiating the β^2_{eff} equation. For core-shell particles, we tried to derive a β^2_{eff} equation similar to Equation 12, however, we were not able to formulate an equation simply involving parameters $\omega_e t_{mw}$, β_c and β_d. Therefore, we employed numerical simulations to observe the frequency effect on the β^2_{eff} for different material parameter combinations. Any material combination is possible. For example, a metallic core with an inorganic shell particles have $\sigma_1 < 1 < \varepsilon_1$ and $\sigma_2 < \varepsilon_2 < 1$. An inorganic core with a semi-conducting polymeric shell particles have $1 < \varepsilon_1 < \sigma_1$, $\varepsilon_2 < 1 < \sigma_2$. Therefore, three classifications, $\sigma_1 = \varepsilon_1$, $\sigma_1 > \varepsilon_1$ and $\sigma_1 < \varepsilon_1$, were made associated with varying σ_2 and ε_2 to discuss the interaction force affected by the frequency. The computational results are listed in Table 1 to 3. The small plot for each condition in the tables shows the relationship between β^2_{eff} and the electric field frequency. If two plots are presented for each condition in the tables, two results will likely appear. The observed results are summarized as

(1) Except for special cases, the $\beta^2_{eff,norm}$ variations with the frequency can be

determined using the values $\beta^2_{c,CS}$ and $\beta^2_{d,CS}$. When $\beta^2_{c,CS} = \beta^2_{d,CS}$, the frequency does not affect the $\beta^2_{eff,norm}$. The $\beta^2_{eff,norm}$ becomes larger as the frequency is higher when $\beta^2_{c,CS} < \beta^2_{d,CS}$. The $\beta^2_{eff,norm}$ becomes smaller as the frequency is higher when $\beta^2_{c,CS} > \beta^2_{d,CS}$.

(2) Since there were no analytical solutions available for the core-shell particles, the exact solutions for the frequency at a reflection point, $\omega_{ei,SC}$, were only observed according to the numerical simulation results. However, Equation 26 can be used for predictions. ω_{ei} for hard core particles was taken as a basis if the particle conductivity became larger using a core material, such as a metallic core. $\omega_{ei,SC}$ for core-shell particles is higher than ω_{ei}. Similarly, if the particle dielectric constant became larger using a core material, $\omega_{ei,SC}$ for core-shell particles is lower than ω_{ei}. Thus, $\omega_{ei,SC} > \omega_{ei}$ if $\sigma_2 < 1 < \varepsilon_2$ and $\omega_{ei,SC} < \omega_{ei}$ if $\sigma_2 > 1 > \varepsilon_2$.

(3) $\beta^2_{eff,norm}$ showed a maximum when $\sigma_1 > \varepsilon_1 > 1$, $\sigma_2 > 1 > \varepsilon_2$ and $\varepsilon_1 > \sigma_1 > 1$, $\varepsilon_2 > 1 > \sigma_2$.

(4) $\beta^2_{eff,norm}$ showed a minimum when $\sigma_1 > 1 > \varepsilon_1$, $\varepsilon_1 > 1 > \sigma_1$ and $\sigma_2 > 1 > \varepsilon_2$, $\varepsilon_2 > 1 > \sigma_2$.

In summary, the influence of the frequency on β^2_{eff} was complicated for core-shell particles. Under certain material combinations, the β^2_{eff} curve appeared as a maximum or a minimum. However, if the changes were not considered within a frequency range, only the β^2_{eff} values at the extremes, a very high and low frequency, were to be known. Equations 22 and 24 were used to solve the β^2_{eff}.

Table 1. Stress responses $\beta^2_{eff,norm}$ versus frequency ω_e for $\sigma_1 = \varepsilon_1$

Condition		$\beta^2_{eff,norm}$ vs ω_e	Condition		$\beta^2_{eff,norm}$ vs ω_e
$\sigma_1 = \varepsilon_1 < 1$	$\sigma_2 = \varepsilon_2 > 1$		$\sigma_1 = \varepsilon_1 > 1$	$\sigma_2 = \varepsilon_2 > 1$	
	$\sigma_2 = \varepsilon_2 < 1$			$\sigma_2 = \varepsilon_2 < 1$	
	$\sigma_2 < \varepsilon_2 < 1$			$\sigma_2 < \varepsilon_2 < 1$	
	$\sigma_2 < 1 < \varepsilon_2$			$\sigma_2 < 1 < \varepsilon_2$	
	$1 < \sigma_2 < \varepsilon_2$			$1 < \sigma_2 < \varepsilon_2$	
	$\sigma_2 > \varepsilon_2 > 1$			$\sigma_2 > \varepsilon_2 > 1$	
	$\sigma_2 > 1 > \varepsilon_2$			$\sigma_2 > 1 > \varepsilon_2$	
	$1 > \sigma_2 > \varepsilon_2$			$1 > \sigma_2 > \varepsilon_2$	

Table 2. Stress responses $\beta^2_{eff,norm}$ versus frequency ω_e for $\sigma_1 > \varepsilon_1$

Condition		$\beta^2_{eff,norm}$ vs ω_e	Condition		$\beta^2_{eff,norm}$ vs ω_e
$\sigma_1 > \varepsilon_1 > 1$	$\sigma_2 = \varepsilon_2 > 1$		$1 > \sigma_1 > \varepsilon_1$	$\sigma_2 = \varepsilon_2 > 1$	
	$\sigma_2 = \varepsilon_2 < 1$			$\sigma_2 = \varepsilon_2 < 1$	
	$\sigma_2 < \varepsilon_2 < 1$			$\sigma_2 < \varepsilon_2 < 1$	
	$\sigma_2 < 1 < \varepsilon_2$			$\sigma_2 < 1 < \varepsilon_2$	
	$1 < \sigma_2 < \varepsilon_2$			$1 < \sigma_2 < \varepsilon_2$	
	$\sigma_2 > \varepsilon_2 > 1$			$\sigma_2 > \varepsilon_2 > 1$	
	$\sigma_2 > 1 > \varepsilon_2$	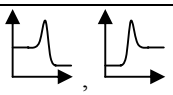		$\sigma_2 > 1 > \varepsilon_2$	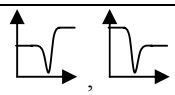
	$1 > \sigma_2 > \varepsilon_2$	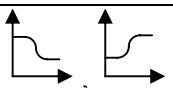		$1 > \sigma_2 > \varepsilon_2$	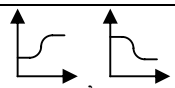
$\sigma_1 > 1 > \varepsilon_1$ and $\beta_c^2 > \beta_d^2$	$\sigma_2 = \varepsilon_2 > 1$	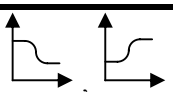	$\sigma_1 > 1 > \varepsilon_1$ and $\beta_c^2 < \beta_d^2$	$\sigma_2 = \varepsilon_2 > 1$	
	$\sigma_2 = \varepsilon_2 < 1$			$\sigma_2 = \varepsilon_2 < 1$	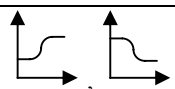
	$\sigma_2 < \varepsilon_2 < 1$			$\sigma_2 < \varepsilon_2 < 1$	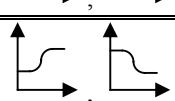
	$\sigma_2 < 1 < \varepsilon_2$	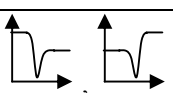		$\sigma_2 < 1 < \varepsilon_2$	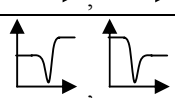
	$1 < \sigma_2 < \varepsilon_2$	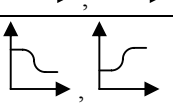		$1 < \sigma_2 < \varepsilon_2$	
	$\sigma_2 > \varepsilon_2 > 1$	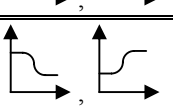		$\sigma_2 > \varepsilon_2 > 1$	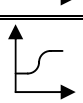
	$\sigma_2 > 1 > \varepsilon_2$	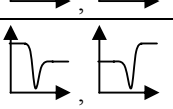		$\sigma_2 > 1 > \varepsilon_2$	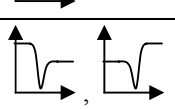
	$1 > \sigma_2 > \varepsilon_2$	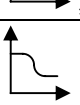		$1 > \sigma_2 > \varepsilon_2$	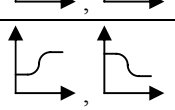

Table 3. Stress responses $\beta^2_{eff,norm}$ versus frequency ω_e for $\sigma_1 < \varepsilon_1$

Condition		$\beta^2_{eff,norm}$ vs ω_e	Condition		$\beta^2_{eff,norm}$ vs ω_e
$\sigma_1 < \varepsilon_1 < 1$	$\sigma_2 = \varepsilon_2 > 1$		$1 < \sigma_1 < \varepsilon_1$	$\sigma_2 = \varepsilon_2 > 1$	
	$\sigma_2 = \varepsilon_2 < 1$			$\sigma_2 = \varepsilon_2 < 1$	
	$\sigma_2 < \varepsilon_2 < 1$			$\sigma_2 < \varepsilon_2 < 1$	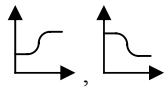
	$\sigma_2 < 1 < \varepsilon_2$	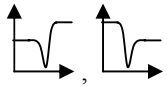		$\sigma_2 < 1 < \varepsilon_2$	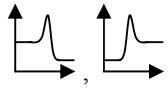
	$1 < \sigma_2 < \varepsilon_2$	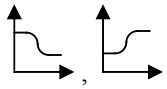		$1 < \sigma_2 < \varepsilon_2$	
	$\sigma_2 > \varepsilon_2 > 1$			$\sigma_2 > \varepsilon_2 > 1$	
	$\sigma_2 > 1 > \varepsilon_2$			$\sigma_2 > 1 > \varepsilon_2$	
	$1 > \sigma_2 > \varepsilon_2$			$1 > \sigma_2 > \varepsilon_2$	
$\sigma_1 < 1 < \varepsilon_1$ and $\beta_c^2 < \beta_d^2$	$\sigma_2 = \varepsilon_2 > 1$	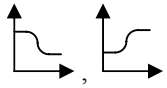	$\sigma_1 < 1 < \varepsilon_1$ and $\beta_c^2 > \beta_d^2$	$\sigma_2 = \varepsilon_2 > 1$	
	$\sigma_2 = \varepsilon_2 < 1$			$\sigma_2 = \varepsilon_2 < 1$	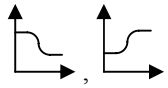
	$\sigma_2 < \varepsilon_2 < 1$			$\sigma_2 < \varepsilon_2 < 1$	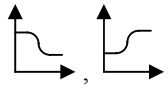
	$\sigma_2 < 1 < \varepsilon_2$	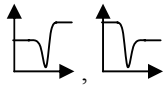		$\sigma_2 < 1 < \varepsilon_2$	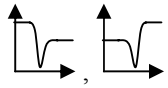
	$1 < \sigma_2 < \varepsilon_2$	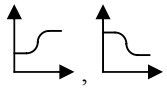		$1 < \sigma_2 < \varepsilon_2$	
	$\sigma_2 > \varepsilon_2 > 1$	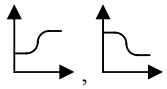		$\sigma_2 > \varepsilon_2 > 1$	
	$\sigma_2 > 1 > \varepsilon_2$	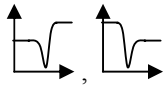		$\sigma_2 > 1 > \varepsilon_2$	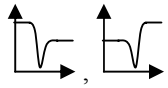
	$1 > \sigma_2 > \varepsilon_2$			$1 > \sigma_2 > \varepsilon_2$	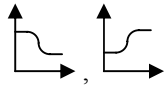

This paper emphasizes the influence of the electric field frequency on the stress response of an ERF. Therefore, Tables 1 to 3 only showed the interaction force trends affected by the frequency. The β_{eff}^2 values are not listed in detail. For the effects of σ_1, ε_1, σ_2, ε_2 combinations on the β_{eff}^2, they were discussed in our publications. Here, we summarize the conclusions from those publications.

Consider the extreme at a high frequency. The β_{eff}^2 is independent of σ_1 and σ_2.

(1) $\varepsilon_1 > 1$:

The computed value of β_{eff}^2 for core-shell particles is larger than that for hard core particles if $\varepsilon_2 < 1$. But if $\varepsilon_2 > 1$, the computed value of β_{eff}^2 for core-shell particles is smaller than that for hard core particles.

(2) $\varepsilon_1 < 1$:

The calculated value of β_{eff}^2 for core-shell particles is larger than that for hard core particles if $\varepsilon_2 > 1$. But if $\varepsilon_2 < 1$, the calculated value of β_{eff}^2 for core-shell particles is smaller than that for hard core particles.

Consider the extreme at a low frequency or under a DC field. The β_{eff}^2 is independent of ε_1 and ε_2.

(1) $\sigma_1 > 1$:

The computed value of β_{eff}^2 for core-shell particles is larger than that for hard core particles if $\sigma_2 < 1$. But if $\sigma_2 > 1$, the computed value of β_{eff}^2 for core-shell particles is smaller than that for hard core particles.

(2) $\sigma_1 < 1$:

The calculated value of β_{eff}^2 for core-shell particles is larger than that for hard core particles if $\sigma_2 > 1$. But if $\sigma_2 < 1$, the calculated value of β_{eff}^2 for core-shell particles is smaller than that for hard core particles.

IV. CONCLUSIONS

The frequency at the reflection point, ω_{ei}, in the stress versus frequency curves is useful in choosing the external electrical field frequency range for ERF particles applications. For hard core particles, we computed ω_{ei} using the particle electrical parameters and the surrounding medium. However, the numerical computations were performed to solve the ω_{ei} for core-shell particles.

The stress responses to the frequency of core-shell particles in ERF were much more complicated than that for hard core particles. Under certain parameter combinations, a maximum or a minimum appeared. Such complexity can be ignored if the intended frequency is not used to control the ERF stress response. To choose a DC or AC field for the external electric field, we must calculate $\beta_{c,CS}^2$ and $\beta_{d,CS}^2$ and then compare these two values. If $\beta_{c,CS}^2 > \beta_{d,CS}^2$, a DC field is a better choice.

REFERENCES

[1] Winslow W. M., "Induced Fibration of Suspensions," Journal of Applied Physics, Vol. 20, No. 3, pp. 1137-1140, 1949.

[2] Cho, M. S., Cho, Y. H., Choi, H. J., and Jhon, M. S., "Synthesis and Electrorheological Characteristics of Polyaniline-Coated Poly(methyl methacrylate) Microsphere: Size Effect," Langmuir, Vol. 19, No. 14, pp. 5875-5881, 2003.

[3] Hao, T., "Electrorheological Suspensions," Advances in Colloid and Interface Science, Vol. 97, No. 1, pp. 1-35, 2002.

[4] Ahn, K. H. and Klingenberg, D. J., "Relaxation of Polydisperse Electrorheological Suspensions," Journal of Rheology, Vol.38, No.3, pp. 713-741, 1994.

[5] Wan, J. T. K., Gu, G. Q., and Yu, K. W., "Nonlinear ER Effects in an AC Applied Field," Computer Physics Communications, Vol. 142, No. 2, pp. 457-463, 2001.

[6] Klingenberg, D. J. and Zukoski, C. F., "Studies on the Steady-Shear Behavior of Electrorheological Suspensions," Langmuir, Vol. 6, No. 1, pp. 15-24, 1990.

[7] Chen, Y. A., Sprecher, F., and Conrad, H., "Electrostatic Particle-Particle Interactions

in Electrorheological Fluids," Journal of Applied Physics, Vol.70, No.11, pp.6796-6803, 1991.

[8] Davis, L. C., "Polarization Forces and Conductivity Effects in Electrorheological Fluids," Journal of Applied Physics, Vol. 72, No. 4, pp. 1334-1340, 1992.

[9] Yu, K. W. and Wan, J. T. K., "Interparticle Force in Polydisperse Electrorheological Fluids," Computer Physics Communications, Vol. 129, No. 1, pp. 177-184, 2000.

[10] Hao, T., "Electrorheological Fluids," Advanced Materials, Vol. 13, No. 24, pp. 1847-1857, 2001.

[11] Trlica, J., Saha, P., Quadrat, O., and Stejskal, J., "Electrorheology of Polyaniline-Coated Silica Particles in Silicone Oil," Journal of Physics D: Applied Physics, Vol. 33, No. 15, pp. 1773-1780, 2000.

[12] Kuramoto, N., Yamazaki, M., Nagai, K., Koyama, K., Tanaka, K., Yatsuzuka, K., and Higashiyama, Y., "Electrorheological Property of a Polyaniline-Coated Silica Suspension," Thin Solid Films, Vol. 239, No. 1, pp. 169-171, 1994.

[13] Stejskal, J., Quadrat, O., Sapurina, I., Zemek, J., Drelinkiewicz, A., Hasik, M., Krivka, I., and Prokeš, J., "Polyaniline-coated Silica Gel," European Polymer Journal, Vol. 38, No 4, pp. 631-637, 2002.

[14] Cho, M. S., Choi, H. J., Kim, K. Y., and Ahn, W. S., "Synthesis and Characterization of Polyaniline /Mesoporous SBA-15 Nanocomposite," Macromolecular Rapid Communications, Vol. 23, No. 12, pp. 713-716, 2002.

[15] Choi, H. J., Cho, M. S., and Ahn, W. S., "Synthesis of Polyaniline/MCM-41 Nanocomposite and Its Electrorheological Property," Synthetic Metals, Vol. 135, No. 4, pp. 711-712, 2003.

[16] Lengálová, A., Pavlínek, V., Sáha, P., Stejskal, J., and Quadrat, O., "Electrorheology of Polyaniline-coated Inorganic Particles in Silicone Oil," Journal of Colloid and Interface Science, Vol. 258, No. 1, pp. 174-178, 2003.

[17] Kuramoto, N., Yamazaki, M., Nagai, K., Koyama, K., Tanaka, K., Yatsuzuka, K., and Higashiyama, Y., "The Electrorheological Property of a Polyaniline-coated Copolystyrene Particle Suspension," Rheologica Acta, Vol.34, No.3, pp. 298-302, 1995.

[18] Park, M. K., Onishi, K., Locklin, J., Caruso, F., and Advincula, R. C., "Self-Assembly and Characterization of Polyaniline and Sulfonated Polystyrene Multilayer-Coated Colloidal Particles and Hollow Shells," Langmuir, Vol. 19, No. 20, pp. 8550-8554, 2003.

[19] Davis, L. C., "The Metal-particle/Insulating Oil System: An Ideal Electrorheological Fluid," Journal of Applied Physics, Vol. 73, No. 2, pp. 680-683, 1993.

[20] Guo, H. X., Zhao, X. P., Ning, G. H., and Liu, G. Q., "Synthesis of Ni/Polystyrene /TiO_2 Multiply Coated Microspheres," Langmuir, Vol. 19, No. 12, pp. 4884-4888, 2003.

[21] Dukain, S. S., "Dielectric Properties of Disperse Systems," Surface and Colloid Science, Vol. 3, No. 1, pp. 83-165, 1970.

[22] Khusid, B. and Acrivos, A., "Effects of Conductivity in Electric-field-induced Aggregation in Electrorheological Fluids," Physical Review E, Vol. 52, No. 2, pp. 1669-1689, 1995.

[23] Block, H. and Kelly, J. P., "Electro-rheology," Journal of Physics D: Applied Physics, Vol. 21, No. 3, pp. 1661-1677, 1988.

[24] Gast, A. P. and Zukoski, C. F., "Electrorheological Fluids as Colloidal Suspensions," Advance in Colloid and interface Science, Vol. 30, No. 1, pp. 153-202, 1989.

[25] Weiss, K. D., Carlson, J. D., and Coulter, J. P., "Material Aspects of Electrorheological Systems," Journal of Intelligent Material Systems and Structures, Vol. 5, No. 1, pp. 13-34, 1993.

[26] Kim, Y. D. and Klingenberg, D. J., "Surfactant-activated Electrorheological Suspensions," Polymer Preprints, Vol. 35, No. 2, pp. 398-390, 1994.

APPENDIX

The derivation of Equation (2) is stated as follows:

$$p = 4\pi\varepsilon_f \beta b^3 E_o \tag{2}$$

A dipole moment along the z direction is starting at the origin. An electric potential at a point with a distance r from the origin can be expressed as Equation (A1).

$$V^p = \frac{1}{4\pi\varepsilon_f}\frac{p}{r^2}\cos\theta \tag{A1}$$

An insulating material with a dielectric ε_p and a radius b is immersed in a homogeneous dielectric fluid with a dielectric ε_f. An external electric field is $E_o\mathbf{z}$ applied. The potential must satisfy $\nabla^2 V = 0$ in the liquid zone and within the sphere. The boundary conditions are

$$\begin{aligned} &r \to \infty \quad V^I = -E_o r\cos\theta \\ &r = b \quad V^I = V^{II}, \quad \varepsilon_f \nabla V^I \cdot n = \varepsilon_p \nabla V^{II} \cdot n \end{aligned} \tag{A2}$$

The electric potential in the liquid zone can be derived as

$$V^I(r,\theta) = -E_o r\cos\theta + \frac{\beta b^3}{r^2}E_o\cos\theta \tag{A3}$$

The potential consists of two parts. The first part is due to the external field effect and the second part is due to the polarization induced dipole. Comparing $\frac{\beta b^3}{r^2}E_o\cos\theta$ and Equation (A1), the solid particle equivalent dipole under the application of an electric field can be expressed as

$$p = 4\pi\varepsilon_f \beta b^3 E_o \tag{2}$$